Railway Sciences

37

Parameter influence analysis and optimization of wheel–rail creepage characteristics in high-speed railway curves

Bolun An, Jiapeng Liu, Guang Yang, Feng shou Liu, Tong Shi and Ming Zhai

Metals and Chemistry Research Institute, China Academy of Railway Sciences Corporation Limited, Beijing, China

Received 27 December 2024
Revised 3 January 2025
Accepted 3 January 2025

Abstract

Purpose – To investigate the influence of vehicle operation speed, curve geometry parameters and rail profile parameters on wheel–rail creepage in high-speed railway curves and propose a multi-parameter coordinated optimization strategy to reduce wheel–rail contact fatigue damage.

Design/methodology/approach – Taking a small-radius curve of a high-speed railway as the research object, field measurements were conducted to obtain track parameters and wheel–rail profiles. A coupled vehicle-track dynamics model was established. Multiple numerical experiments were designed using the Latin Hypercube Sampling method to extract wheel-rail creepage indicators and construct a parameter-creepage response surface model.

Findings – Key service parameters affecting wheel–rail creepage were identified, including the matching relationship between curve geometry and vehicle speed and rail profile parameters. The influence patterns of various parameters on wheel–rail creepage were revealed through response surface analysis, leading to the establishment of parameter optimization criteria.

Originality/value – This study presents the systematic investigation of wheel–rail creepage characteristics under multi-parameter coupling in high-speed railway curves. A response surface-based parameter-creepage relationship model was established, and a multi-parameter coordinated optimization strategy was proposed. The research findings provide theoretical guidance for controlling wheel–rail contact fatigue damage and optimizing wheel–rail profiles in high-speed railway curves.

Keywords High-speed railway, Curve track, Wheel–rail creepage, Parameter analysis, Response surface methodology, Optimization design

Paper type Research paper

1. Introduction

The stability and durability requirements for busy high-speed railway lines in China are extremely demanding. The operational environment of high-speed railways is complex and varied, involving multiple vehicle types, different wheel-rail profiles, and diverse operating conditions. Particularly in sections with complex terrain featuring long steep grades, frequent traction/braking operations are required. These factors lead to significant variations in the running state of high-speed trains in curved sections, directly affecting both curve negotiation performance and wheel-rail creepage characteristics.

This study was sponsored by the National Natural Science Foundation of China (Grant No. 52405443), the Technology Research and Development Plan of China Railway (Grant No. N2023G063) and the Fund of China Academy of Railway Sciences Corporation Limited (Grant No. 2023YJ054).

Railway Sciences
Vol. 4 No. 1, 2025
pp. 37-51
Emerald Publishing Limited
e-ISSN: 2755-0915
p-ISSN: 2755-0907
DOI 10.1108/RS-12-2024-0056

When curve negotiation conditions are poor, wheel-rail creepage increases significantly. This not only accelerates the formation and development of contact fatigue damage but can also lead to rail surface temperature elevation under traction/braking actions, causing microstructural changes in rail material and forming thin layers of brittle martensite. Due to the extremely poor toughness of martensitic structure, cracks rapidly initiate and propagate under rolling contact fatigue, resulting in thermo-mechanical fatigue damage. Such problems not only compromise operational safety but also significantly reduce rail service life. Therefore, controlling wheel-rail creepage in curved sections is crucial for enhancing vehicle-track system performance and mitigating wheel-rail fatigue damage, with understanding the relationship between curve operation parameters and wheel-rail creepage being a key strategy.

Wheel-rail creepage and its associated phenomena have been extensively studied through various approaches. (Vollebregt, Six, & Polach, 2021) conducted a comprehensive survey on wheel-rail creep forces modeling, emphasizing the significant progress in understanding tribological aspects over the past two decades, particularly focusing on surface conditions' influence on creep force characteristics. To validate theoretical models experimentally, (Alonso, Guiral, Baeza, & Iwnicki, 2014) developed a scaled test bench to characterize wheel-rail contact forces, revealing discrepancies with Kalker's simplified theory and analyzing the effects of various contaminants. For the investigation of specific scenarios, (Lei & Wang, 2021) established a vehicle-track coupled dynamic model to study contact and creep characteristics under harmonic corrugation excitation, finding that wave depth significantly affects longitudinal and transverse creepage. (Cui *et al.*, 2015) investigated rail corrugation on curved tracks using finite element analysis, demonstrating that contact angle and saturated creep force direction significantly influence self-excited vibration. To address the limitations of traditional algorithms, (Spiryagin, Polach, & Cole, 2013) proposed a modified version of Kalker's FASTSIM algorithm for more accurate creep force modeling at large creepages, particularly for high-power traction vehicles.

Recent high-speed railway research has focused on more specific aspects of wheel-rail interaction. (Yin, Zhao, Huang, Wen, & Jin, 2024) employed finite element analysis to study creep curves under high-speed conditions up to 500 km/h, particularly examining the influence of middle/high-frequency vibrations. (Ren, Xie, & Iwnicki, 2012) investigated short pitch corrugation effects on longitudinal creep forces using Kalker's variational method, developing transfer functions for non-steady state analysis. (Zhuang, Yu, & Xiaolei, 2019) compared FASTSIM and CONTACT algorithms for creep force calculation, finding that CONTACT provides more accurate results under transient rolling conditions. (Hu *et al.*, 2020) studied the influence of wheel/rail hardness ratios and creepage on wear and rolling contact fatigue, while (Chang, Chen, Cai, & Wang, 2024) investigated adhesion characteristics under large creepage and water conditions at high speeds. Recent optimization efforts by (Liu, Mei, & Bruni, 2016; Wu, Xiao, An, Wu, & Shen, 2022) have focused on improving wheel-rail profile design for better adhesion and studying dynamic interactions under low adhesion conditions, providing valuable insights for practical applications in high-speed railways.

Although existing research has extensively investigated wheel-rail creepage mechanisms and control measures, the sensitivity of wheel-rail creepage to various parameters has not been systematically revealed, making it difficult to propose precise and effective parameter optimization schemes. Considering field conditions, parameters such as rail profiles, curve superelevation, and operating speed are adjustable, while curve radius is generally fixed. Therefore, taking a specific high-speed railway line as a case study, this paper employs numerical experiments to systematically analyze the quantitative relationships between wheel-rail creepage and the aforementioned service parameters. The study aims to propose parameter optimization strategies for minimizing wheel-rail creepage, providing theoretical guidance for reducing wheel-rail contact fatigue damage, improving wheel-rail service performance, and optimizing maintenance schemes.

2. Rail service condition testing and analysis

A section of a high-speed railway with a small-radius curve has been experiencing significant wheel-rail creep in recent years, leading to extensive contact fatigue damage and thermo-mechanical fatigue damage. In severe cases, the depth of the cracks has exceeded 6 mm, necessitating rail replacement. This paper takes this section as a case study for analysis.

2.1 Railway line parameters

The primary operating vehicles in this section are the CRH380B and CR400BF trains, with a curve negotiation speed of 200 km/h and a radius of 2,200 m. The actual superelevation is set at 175 mm, resulting in an under-superelevation of approximately 40 mm when vehicles pass through. In addition, the line includes gradients of −20% and +20%, along with multiple tunnels. Therefore, the theoretical model in this study also takes into account the impact of gradients and aerodynamic drag within the tunnels.

2.2 Measured rail profile

On-site rail profile measurements were conducted, as shown in Figure 1. Compared to the standard 60N profile, the measured profiles generally exhibited a positive deviation. The largest positive deviation was observed on the high rail, reaching up to 1 mm, while the low rail showed a smaller deviation, with a maximum positive deviation of approximately 0.7 mm.

3. Numerical experiment design and analysis methods

3.1 Vehicle-track coupled dynamics analysis model

The vehicle system is modeled based on multi-body dynamics theory, where all major components (car body, frame, wheelsets, and axle boxes) are considered as rigid bodies with six degrees of freedom. The wheelset dynamics are governed by nonlinear differential equations that account for the coupled lateral-yaw motion, which is crucial for analyzing vehicle curving performance. The suspension system is modeled in detail, incorporating both primary and secondary suspensions. The primary suspension, consisting of springs and vertical dampers, mainly handles wheel-rail contact forces and provides basic vehicle stability. The secondary suspension, including air springs, lateral dampers, yaw dampers, traction rods, and lateral stops, ensures ride comfort and guides the vehicle through curves. These

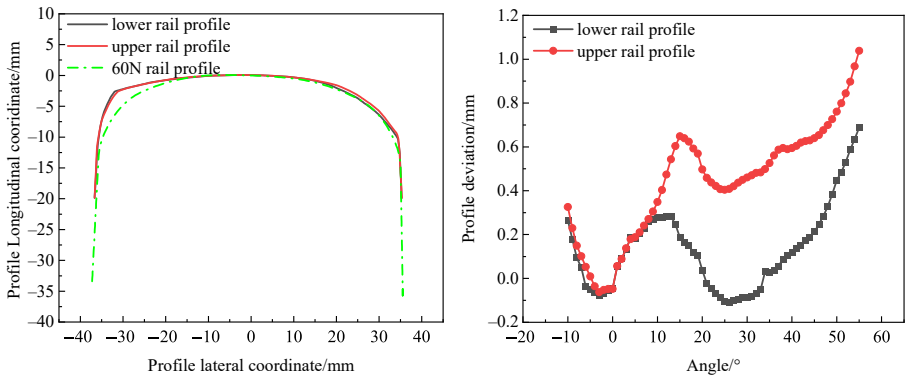

Measured rail profile

(a)

Deviation between measured profile and 60N profile

(b)

Source(s): Authors' own work

Figure 1. Measured rail profile and deviation analysis

suspension elements are characterized by nonlinear force-displacement relationships to capture their actual mechanical behavior. The comprehensive modeling of these nonlinear coupling effects between structural components enables the simulation model to accurately represent the complex dynamic behavior of the vehicle system, particularly during curve negotiation. (Wang, An, Ma, Wang, & Liu, 2024)

The wheel-rail contact calculation is based on non-Hertzian contact theory and Kalker's FASTSIM algorithm. In curved track sections, due to the use of measured wheel-rail profile data and the presence of wheelset lateral displacement and rotation angle, the contact characteristics between wheel and rail deviate significantly from traditional elliptical Hertzian contact, exhibiting non-elliptical characteristics in contact area shape and stress distribution. Therefore, non-Hertzian contact theory is adopted to achieve more accurate contact analysis. The calculation process primarily consists of three aspects: Contact point coordinate determination, contact mechanics computation (contact forces, creepage, etc.) and contact patch analysis (contact stress, creep stress, sliding velocity distribution, etc.) (Ayasse & Chollet, 2005; Junjun, Fu, & Yunhua, 2011).

Considering the presence of gradients in actual track conditions, this railway line model includes gradients of −20% and +20% to analyze their influence on wheel-rail creepage. The curve section has a radius of 2,200 m with a superelevation of 175 mm. The track parameters used in the simulation are shown in Figure 2.

Given the presence of multiple tunnels along this section, the aerodynamic resistance effects on longitudinal wheel-rail creepage during tunnel entry and exit are incorporated into the simulation. According to the reference study (Haoran, 2022), the maximum aerodynamic resistance in tunnels exhibits a positive correlation with speed, following the fitting formula:

$$F = 0.4024v^2 \tag{1}$$

The analysis reveals that aerodynamic resistance is proportional to the square of velocity. In the simulation, this is applied as a longitudinal resistance force directly acting on the vehicle body when entering curved sections. The relationship between aerodynamic resistance and vehicle operating speed is illustrated in Figure 3.

The results demonstrate that under aerodynamic resistance, the vehicle speed gradually decreases, effectively acting as a low-intensity braking force. After applying resistance over 1,600 m, the train speed reduces to 166 km/h.

3.2 Numerical experiment design and analysis methods

During vehicle operation, wheelset lateral displacement occurs under centrifugal forces or track excitation, causing the wheelset centerline to deviate from the track centerline. This

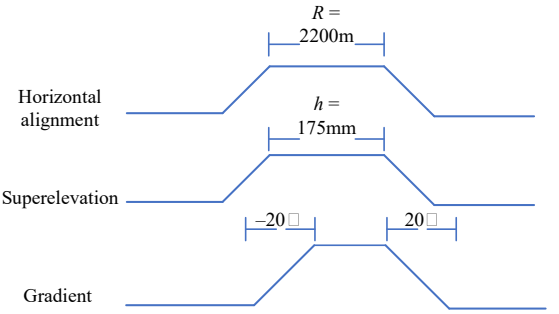

Source(s): Authors' own work

Figure 2. Track parameters input for modeling

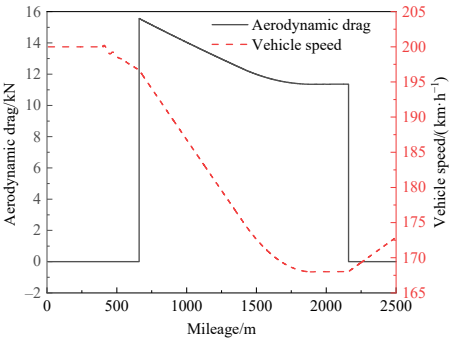

Source(s): Authors' own work

Figure 3. Correlation between aerodynamic resistance and vehicle operating speed

deviation results in varying rolling radius at the left and right wheel contact points. Since the wheelset is a rigid body with a constant angular velocity at any given moment, this creates a mismatch between the actual and required linear velocities at the wheel-rail contact points, leading to wheel-rail creepage. The magnitude of wheel-rail creepage directly correlates with the proportion of slip area within the contact zone. When the entire contact zone becomes a slip area, the wheel-rail contact transitions to pure sliding state. Factors affecting wheel-rail creepage include rolling radius difference between left and right wheels, wheel-rail contact area, wheel-rail adhesion saturation, and wheel-rail creepage.

The study of the effects of curve alignment parameters and wheel-rail profiles essentially involves single/multi-factor influence pattern analysis. Based on relevant standards and operational experience, these parameters have defined upper and lower limits. Therefore, numerical experiment design and analysis methods are employed to investigate their effects on wheel-rail creepage.

3.2.1 Numerical experiment design method. This research, being based on numerical modeling, allows for the design of numerous test conditions to thoroughly examine parameter randomness within their numerical ranges. The Latin Hypercube Sampling (LHS) method is selected for experimental design, as it is particularly suitable for sampling in high-dimensional spaces (Helton & Davis, 2003).

The fundamental principle of LHS involves dividing each input parameter's range into equal intervals and ensuring each interval is sampled only once. This approach reduces correlation between samples and achieves good experimental accuracy with relatively few test points.

To enhance the experimental design's representativeness, specific parameter value designs are incorporated into the LHS sampling: Starting point (minimum value): Ensures inclusion of minimum parameter values to understand their effects under extreme conditions. Midpoint (median value): Introduces median parameter values to cover the middle region of the parameter space, which is often sensitive for nonlinear phenomena. Endpoint (maximum value): Ensures inclusion of maximum parameter values to evaluate their effects at upper limits.

3.2.2 Experimental results analysis method. Response Surface Methodology (RSM) is employed to fit the response indicators and extract meaningful information from the experimental data. RSM is a statistical technique for optimizing and exploring relationships between response variables and input variables in multivariate systems through mathematical modeling (Khuri & Mukhopadhyay, 2010).

RSM typically employs quadratic polynomial models to represent system responses. For a system with k input variables $x_1, x_2, x_3, x_4, ..., x_k$, the response variable y can be expressed as:

$$y = \beta_0 + \sum_{i=1}^{k} \beta_i x_i + \sum_{i=1}^{k} \beta_{ii} x_i^2 + \sum_{1 \le i \le j \le k} \beta_{ij} x_i x_j + \varepsilon$$

where $\beta_0, \beta_i, \beta_{ii}, \beta_{ij}$ are regression coefficient, ε is the error item.

Once established, the model allows for optimal response variable points (typically maxima or minima) to be determined through derivative analysis, or response surface shapes to be analyzed through contour plots. In this study, model structure and parameters are adjusted to maximize the coefficient of determination (R^2), using this as the criterion for optimal response surface selection. The final response surface model enables accurate prediction and analysis of result indicators within the experimental parameter range.

4. Design of numerical experiment and results analysis

4.1 Influences of curve geometry and operating parameters on wheel-rail creepage

Based on actual track parameters, this study proposes an integrated framework to investigate the influence of curve alignment-vehicle operation parameter matching on wheel-rail creepage, using superelevation, operating speed, and curve radius as analysis parameters. This systematic approach enables comprehensive evaluation of wheel-rail interaction under complex field conditions. The measured rail profiles and worn wheel profiles are used.

The curve section has a radius of 2,200 m and a superelevation of 175 mm, corresponding to an equilibrium speed of 180 km/h. In the numerical experiments, two scenarios are considered based on parameter adjustability: vehicle operating speed (excess/deficient superelevation) and the combination of vehicle operating speed and curve superelevation. This design allows for both single-factor and multi-factor analysis of operational parameters. Latin Hypercube Sampling is employed for test case design.

4.1.1 Speed variation only. For the operating speed parameter range design, given fixed curve superelevation and radius, the parameters can be converted to excess/deficient superelevation during vehicle passage. The excess/deficient superelevation range is set from −100 mm (deficient superelevation) to 100 mm (excess superelevation). Test cases are designed using Latin Hypercube Sampling, as shown in Figure 4.

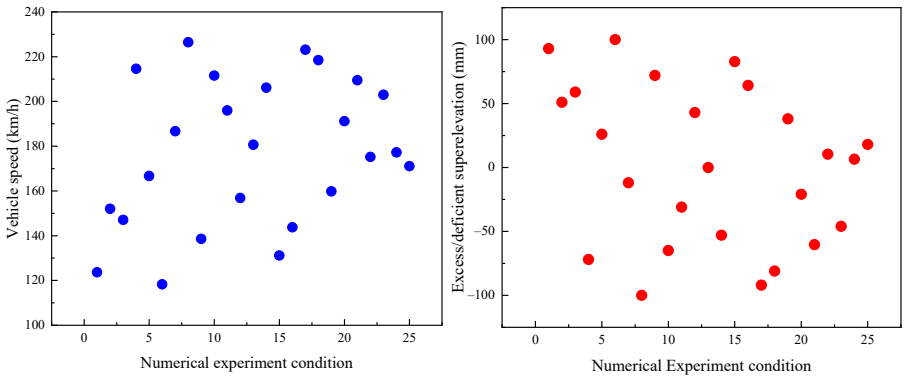

Source(s): Authors' own work

Figure 4. Numerical experiment condition

Considering the close relationship between wheel-rail creepage and indicators such as rolling radius difference and wheel-rail adhesion saturation, these two indicators are first extracted and analyzed, as shown in Figure 5a and 5b.

The longitudinal and lateral creepage are extracted, with results shown in Figure 5c and 5d. The positive and negative signs only indicate the direction of creepage - positive indicates that the creepage direction is the same as the wheel's forward direction, while negative indicates the opposite. The lateral creepage shows a relatively monotonic trend, increasing with decreasing deficient superelevation and increasing excess superelevation. The longitudinal creepage reaches its minimum value of approximately 0.14% at a deficient superelevation of about 65 mm, like the patterns observed in rolling radius difference and wheelset lateral displacement.

It can be observed from Figure 6 that the wheel-rail normal contact stress gradually decreases with decreasing deficient superelevation or increasing excess superelevation, stabilizing when the deficient superelevation reaches about 60 mm. This is a normal phenomenon, as larger deficient superelevation inherently leads to greater wheel-rail forces on the curve's outer rail, resulting in increased stress.

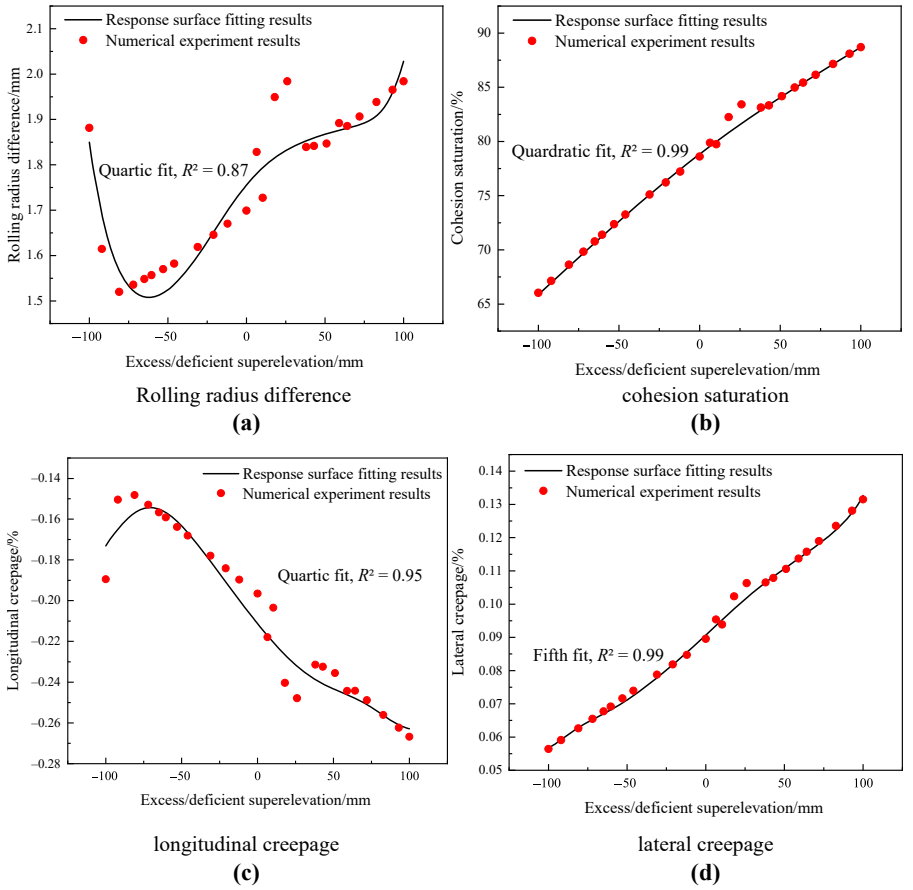

Source(s): Authors' own work

Figure 5. Index of wheel-rail creep

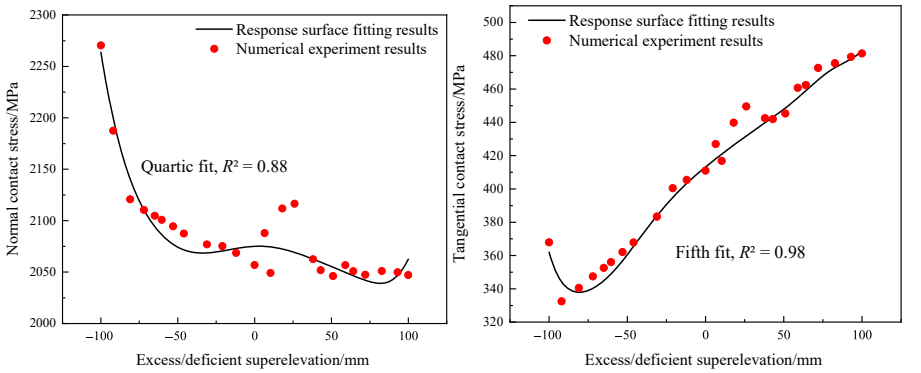

Normal wheel-rail contact stress
(a)

Tangential wheel-rail contact stress
(b)

Source(s): Authors' own work

Figure 6. Wheel-rail contact stress

Furthermore, the wheel-rail tangential contact stress reaches its minimum of approximately 348 MPa at 80 mm deficient superelevation, representing a 7% reduction compared to 100 mm deficient superelevation and a 42% reduction compared to 100 mm excess superelevation.

4.1.2 Combined speed and superelevation variation. This section further considers superelevation variation. With fixed curve radius, the numerical experiment parameters can be converted to excess/deficient superelevation during vehicle passage. The experimental scheme covers vehicle operating speeds from 100 to 230 km/h and curve superelevation from 100 to 175 mm, as shown in Figure 7.

The rolling radius difference and wheel-rail adhesion saturation during curve negotiation were extracted, with results shown in the Figure 8. When the deficient superelevation exceeds 100 mm, the rolling radius difference shows an inflection point and increases rapidly. Its minimum value occurs within the deficient superelevation range of 50–80 mm.

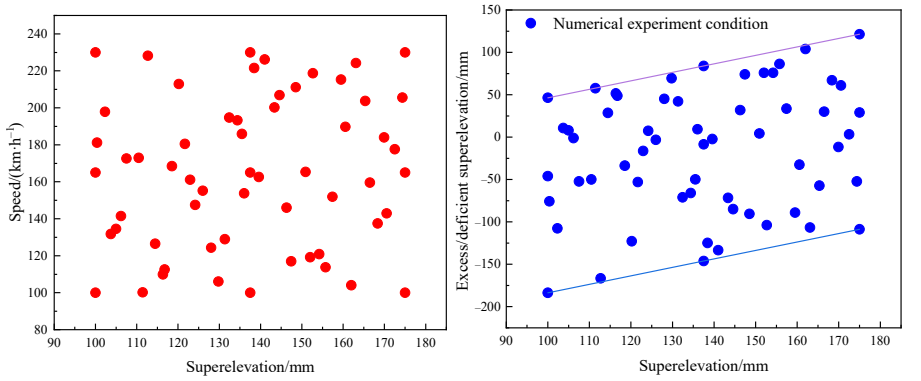

Superelevation-speed
(a)

Superelevation-excess/deficient superelevation
(b)

Source(s): Authors' own work

Figure 7. Numerical experiment condition

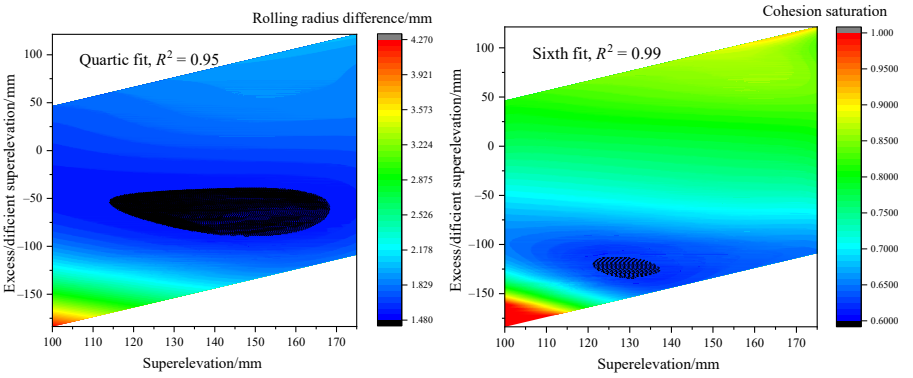

rolling radius difference

(a)

wheel-rail cohesion saturation

(b)

Source(s): Authors' own work

Figure 8. Wheel-rail contact rolling radius difference and cohesion saturation

Correspondingly, the wheel-rail adhesion saturation also maintains relatively low values in this range, though its minimum value appears near 100 mm deficient superelevation. Under excess superelevation conditions and when deficient superelevation exceeds 120 mm, the wheel-rail adhesion saturation shows a significant increasing trend.

The wheel-rail creepage results are extracted as shown in Figure 9. The results indicate that under varying superelevation, the minimum longitudinal creepage consistently occurs within the deficient superelevation range of 50–80 mm, corresponding to a relatively low lateral creepage of around 0.06%.

Contact stress calculations (shown as Figure 10) show that superelevation and excess/deficient superelevation variations have minimal overall impact on normal contact stress. When superelevation deficiency is within 50-80 mm, tangential stress reaches its minimum

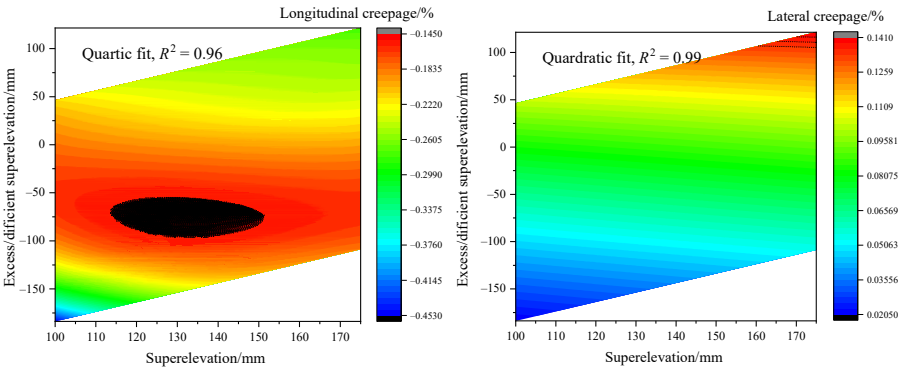

Longitudinal creepage

(a)

Lateral creepage

(b)

Source(s): Authors' own work

Figure 9. Wheel-rail creepage

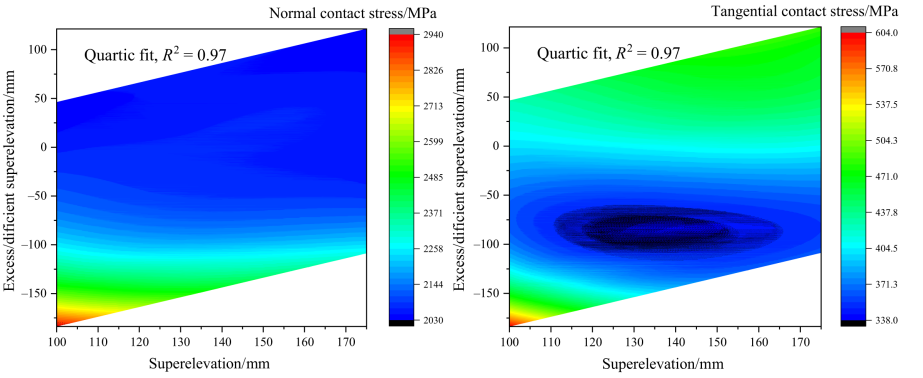

Source(s): Authors' own work

Figure 10. Wheel-rail contact stress

below 350 MPa, representing approximately a 40% reduction compared to the maximum value of 600 MPa.

Overall, both excess superelevation and large deficient superelevation lead to poor wheel-rail contact relationships in curved sections. A superelevation deficiency of 50–80 mm provides optimal wheel-rail adhesion performance and minimal tangential stress.

4.2 Influences of profile configuration on wheel-rail creepage

Rail profile variations significantly influence wheel-rail creepage. Changes in wheel-rail profile matching affect wheelset lateral displacement, rolling radius difference during curve negotiation, and wheel-rail contact area, all which impact wheel-rail creepage and tangential stress. A novel parameterization approach is proposed to analyze the influence patterns of profile variations on wheel-rail creepage. Based on practical rail grinding processes, the profiles are parameterized using two key parameters derived from the 60N profile: rail profile angle (normal angle) and deviation, as shown in Figure 11. This approach enables direct quantification of how actual rail maintenance practices affect wheel-rail interaction.

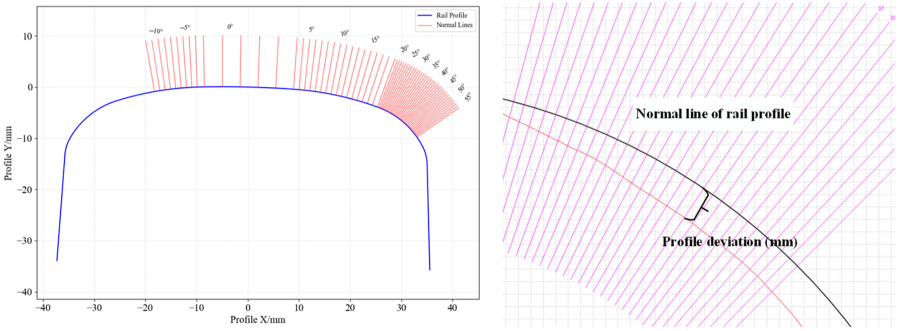

Source(s): Authors' own work

Figure 11. Rail profile parameters

The rail profile deviations approximately follow a normal distribution along the deviation angle, with peak deviation typically occurring at 10–15°. Based on this, the numerical experiment design sets the rail profile deviation angle range as 0–25° and the profile deviation amount range as −0.8 mm (negative deviation) to +0.8 mm (positive deviation). Due to the complex nonlinear relationships between rail profile parameters and wheel-rail creepage indicators, the Latin Hypercube Sampling design includes numerous test cases to accurately describe the influence of profile variations, as shown in Figure 12. The designed numerical calculation cases provide comprehensive coverage of all regions, ensuring strong representativeness.

Using actual alignment and operating speed of the study section as input parameters, the influence patterns of profile deviation on wheel-rail creepage are analyzed. First, the wheel-rail contact rolling radius difference and cohesion saturation are extracted and analyzed, with results shown in Figure 13.

Overall, the influence of profile deviations on wheel-rail contact geometry is complex, with non-monotonic parameter effects. Unlike the influence of curve geometry, the influence of rail profile on wheel-rail relationship exhibits more complexity and nonlinearity, resulting in a lower fitting accuracy of the response surface obtained from numerical experiments compared to the results in Section 4.1. Nevertheless, the overall influence patterns and trends can still be effectively captured. The analysis can be divided into four regions based on profile angle and deviation: positive deviation at rail head, negative deviation at rail head, positive deviation at gauge corner, and negative deviation at gauge corner.

When profile deviation is within ±0.2 mm, the rolling radius difference remains relatively small, generally within 1.4 mm. Significant increases in rolling radius difference occur with negative deviations at the gauge corner or large positive deviations at the rail head center.

Regarding wheel-rail adhesion saturation, lower levels (indicating better adhesion conditions) are observed with negative deviations at the rail head center and positive deviations at the gauge corner, as shown in Figure 14.

Longitudinal creepage is sensitive to profile deviations. The creepage is lower with positive profile deviations and increases rapidly with negative deviations. Lateral creepage shows sensitivity only to large negative deviations at the gauge corner, with an overall low sensitivity to profile deviations.

The wheel-rail contact stress results (shown as Figure 15) show that negative deviations consistently increase wheel-rail contact stress regardless of deviation angle. Within the positive deviation range, when the profile angle is 0–10°, contact stresses show distinct

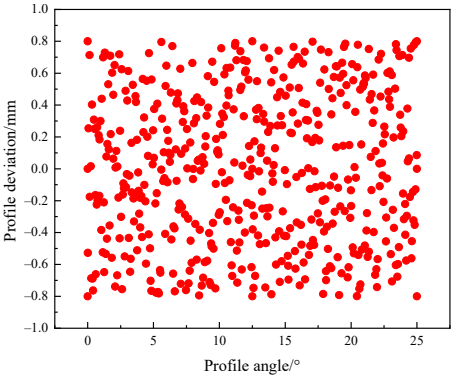

Source(s): Authors' own work

Figure 12. Numerical experiment condition of rail profile parameters

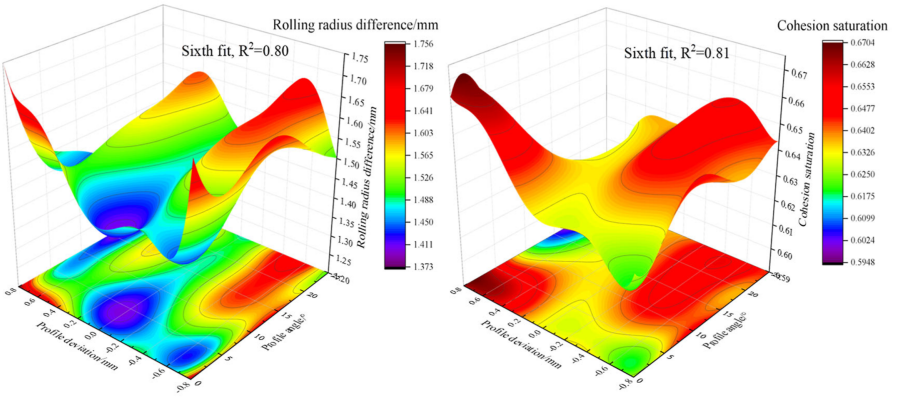

rolling radius difference

(a)

wheel-rail cohesion saturation

(b)

Source(s): Authors' own work

Figure 13. Wheel-rail contact rolling radius difference and cohesion saturation

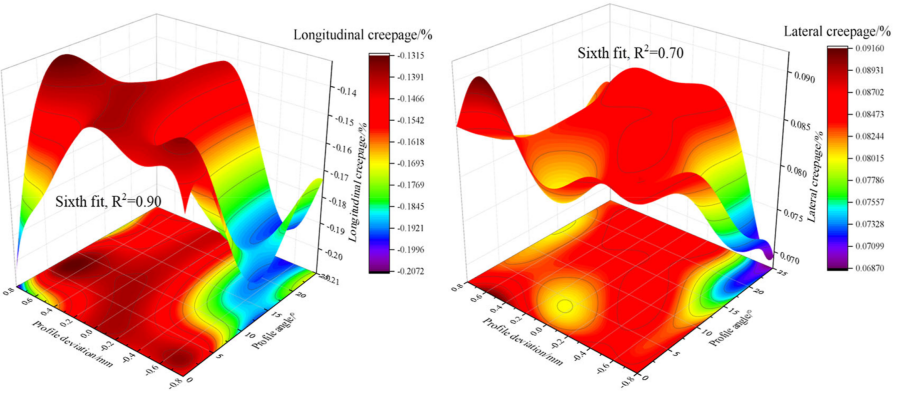

Longitudinal creepage

(a)

Lateral creepage

(b)

Source(s): Authors' own work

Figure 14. Wheel-rail creepage

minima, with normal stress reaching 1,400 MPa and tangential stress reaching 200 MPa, representing reductions of 24% and 30% respectively from peak values, indicating that profile deviations in this region can optimize wheel-rail contact stress.

The relationships between wheel-rail creepage, contact stress, and profile deviations are not uniform, necessitating comprehensive analysis to identify profile characteristics that optimize wheel-rail interaction and reduce rolling contact fatigue. Therefore, adhesion saturation, tangential stress, and longitudinal creepage are considered collectively to determine the optimal region for controlling wheel-rail creepage, as shown in Figure 16.

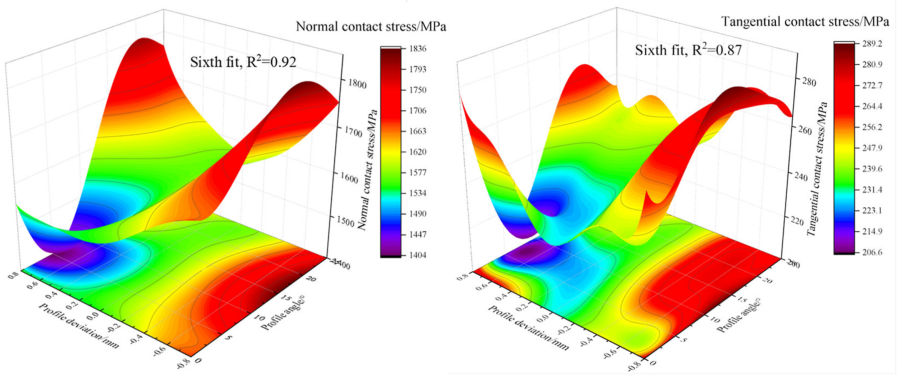

Normal contact stress

(a)

Tangential contact stress

(b)

Source(s): Authors' own work

Figure 15. Wheel-rail contact stress

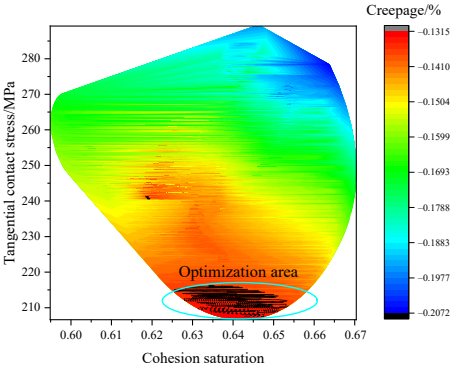

Source(s): Authors' own work

Figure 16. Determination of optimization area

Within the optimization area, wheel-rail adhesion saturation is 0.63–0.65, tangential stress ranges from 200–210 MPa, and longitudinal creepage is −0.13% to −0.14%, corresponding to profile parameters of 5–10° deviation angle and +0.6 mm deviation amount.

Based on the above analysis, two main principles for reducing wheel-rail creepage in high-speed railway curves are established: For curves requiring optimization, appropriate increase in wheel-rail equivalent conicity can reduce wheelset lateral displacement and rolling radius difference during curve negotiation, improving curve passing capability; For sections requiring optimization, enhancement of wheel-rail profile matching conformity can increase contact area and reduce contact stress.

5. Conclusion

Taking a small-radius curve section of a high-speed railway as the research object, this study established a vehicle-track coupled dynamics model based on actual track parameters and vehicle types. The research focused on two major factors affecting wheel-rail creepage: the

matching relationship between curve alignment and operating speed, and rail profile parameters. Using Latin Hypercube Sampling, parametric numerical experiments were designed to investigate the influence patterns of wheel-rail creepage and contact stress indicators. From the perspective of reducing wheel-rail creepage and contact stress, optimal parameter schemes were proposed. The main conclusions are as follows:

(1) A numerical experiment scheme was constructed considering adjustable parameters in actual operations. After the commencement of high-speed railway operations, while curve radius cannot be modified, curve superelevation and vehicle operating speed can be adjusted, and rail profiles can be modified through grinding. Based on this, this study employed Latin Hypercube Sampling to construct numerous numerical experiments, comprehensively examining the effects of these parameter variations on wheel-rail creepage and contact stress.

(2) The relationships between excess/deficient superelevation and wheel-rail creepage and contact stress have been quantified. Results indicate that excess superelevation significantly increases wheel-rail creepage and tangential stress, suggesting that deficient superelevation is a more favorable condition. Through analyzing the correlation between excess/deficient superelevation and wheel-rail creepage, the optimal range of deficient superelevation for curve sections has been identified as 50–80 mm. Within this range, optimal wheel-rail adhesion performance and minimal tangential stress can be ensured. This finding provides theoretical guidance for the design and maintenance of track superelevation in curved sections.

(3) Optimal wheel-rail profile matching parameters have been determined. To reduce wheel-rail creepage in curve sections, the rail profile deviation angle should be concentrated within 5–10°, and the deviation amount should be controlled at approximately +0.6 mm. Under these conditions, wheel-rail adhesion saturation is minimized, while both tangential stress and creepage maintain relatively low levels, effectively reducing the development of wheel-rail rolling contact fatigue.

The research can be applied to track geometry optimization and wheel-rail profile optimization in high-speed railway curve sections, mitigating contact fatigue damage caused by excessive wheel-rail creepage, improving wheel-rail service performance, and extending service life.

The research can be applied to track geometry optimization and wheel-rail profile optimization in high-speed railway curve sections, mitigating contact fatigue damage caused by excessive wheel-rail creepage, improving wheel-rail service performance, and extending service life. The identified parameter influence patterns can guide the development of more targeted rail grinding schedules and maintenance strategies. These findings enable more effective treatment of localized creep issues at curve sections, particularly through optimized grinding profiles. The implementation of these optimization strategies will contribute to enhanced operational efficiency and safety in high-speed railway.

The findings provide theoretical guidance for track geometry design and wheel-rail profile maintenance in high-speed railway curve sections, which helps minimize rolling contact fatigue damage induced by creepage, optimize wheel-rail contact conditions, and extend track component service life. The established parameter sensitivity relationships can be utilized to develop targeted rail grinding specifications and track maintenance standards. The research results facilitate the optimization of local contact conditions at curved sections through rational grinding profile design. These optimization measures contribute to improved vehicle-track interaction performance and operational safety in high-speed railway systems.

References

Alonso, A., Guiral, A., Baeza, L., & Iwnicki, S. (2014). Wheel–rail contact: Experimental study of the creep forces–creepage relationships. *Vehicle System Dynamics*, *52*(sup1), 469–487. doi: 10.1080/00423114.2014.907923.

Ayasse, J. B., & Chollet, H. (2005). Determination of the wheel rail contact patch in semi-Hertzian conditions. *Vehicle System Dynamics*, *43*(3), 161–172. doi: 10.1080/00423110412331327193.

Chang, C., Chen, B., Cai, Y., & Wang, J. (2024). Experimental investigation of high-speed wheel-rail adhesion characteristics under large creepage and water conditions. *Wear*, *540*, 205254. doi: 10.1016/j.wear.2024.205254.

Cui, X. L., Chen, G. X., Yang, H. G., Zhang, Q., Ouyang, H., & Zhu, M. (2015). Effect of the wheel/rail contact angle and the direction of the saturated creep force on rail corrugation. *Wear*, *330*, 554–562. doi: 10.1016/j.wear.2014.12.046.

Haoran, L. (2022). Study on aerodynamic Effects of 400 km/h high-speed trains passing through tunnels. Master degree. Southwest Jiaotong University. CNKI. doi: 10.27414/d.cnki.gxnju.2022.002278.

Helton, J. C., & Davis, F. J. (2003). Latin hypercube sampling and the propagation of uncertainty in analyses of complex systems. *Reliability Engineering & System Safety*, *81*(1), 23–69. doi: 10.1016/S0951-8320(03)00058-9.

Hu, Y., Zhou, L., Ding, H. H., Tan, G., Lewis, R., Liu, Q., . . . Wang, W. (2020). Investigation on wear and rolling contact fatigue of wheel-rail materials under various wheel/rail hardness ratio and creepage conditions. *Tribology International*, *143*, 106091. doi: 10.1016/j.triboint.2019.106091.

Junjun, D., Fu, L. I., & Yunhua, H. (2011). Calculation of wheel wear based on semi-Hertzian contact. *Journal of Southwest Jiaotong University*, *24*(2), 195–200, 1026-1068.

Khuri, A. I., & Mukhopadhyay, S. (2010). Response surface methodology. *Wiley Interdisciplinary Reviews: Computational Statistics*, *2*(2), 128–149. doi: 10.1002/wics.73.

Lei, Z., & Wang, Z. (2021). Contact and creep characteristics of wheel–rail system under harmonic corrugation excitation. *Journal of Vibration and Control*, *27*(17-18), 2069–2080. doi: 10.1177/1077546320953358.

Liu, B., Mei, T. X., & Bruni, S. (2016). Design and optimisation of wheel-rail profiles for adhesion improvement. *Vehicle System Dynamics*, *54*(3), 429–444. doi: 10.1080/00423114.2015.1137958.

Ren, L., Xie, G., & Iwnicki, S. D. (2012). Properties of wheel/rail longitudinal creep force due to sinusoidal short pitch corrugation on railway rails. *Wear*, *284-285*, 73–81. doi: 10.1016/j.wear.2012.02.015.

Spiryagin, M., Polach, O., & Cole, C. (2013). Creep force modelling for rail traction vehicles based on the Fastsim algorithm. *Vehicle System Dynamics*, *51*(11), 1765–1783. doi: 10.1080/00423114.2013.826370.

Vollebregt, E., Six, K., & Polach, O. (2021). Challenges and progress in the understanding and modelling of the wheel–rail creep forces. *Vehicle System Dynamics*, *59*(7), 1026–1068. doi: 10.1080/00423114.2021.1912367.

Wang, P., An, B., Ma, J., Wang, S., & Liu, F. (2024). Theoretical and experimental research on the influence and optimization method of the 60N profile in turnout. *International Journal of Structural Stability and Dynamics*, *24*(13). doi: 10.1142/s0219455424501475.

Wu, B., Xiao, G., An, B., Wu, T., & Shen, Q. (2022). Numerical study of wheel/rail dynamic interactions for high-speed rail vehicles under low adhesion conditions during traction. *Engineering Failure Analysis*, *137*, 106266. doi: 10.1016/j.engfailanal.2022.106266.

Yin, S., Zhao, X., Huang, S., Wen, Z., & Jin, X. (2024). Influence of high-frequency vibrations on the wheel-rail creep curve at high speeds. *Wear*, *536*, 205161. doi: 10.1016/j.wear.2023.205161.

Zhuang, Q. I., Yu, L., & Xiaolei, W. (2019). Comparative study on the theory of creeping theory applied to high speed wheel-rail rolling contact. *Tribology*, *39*(3), 319–329.

Corresponding author
Jiapeng Liu can be contacted at: edisonadd881210@gmail.com